PLA scaffolds production from Thermally Induced Phase Separation: Effect of process parameters and development of an environmentally improved route assisted by supercritical carbon dioxide

Swann Gay, Guillaume Lefebvre, Marie Bonnin, Benjamin Nottelet, Franck Boury, Alain Gibaud, Brice Calvignac

PLA scaffolds production from Thermally Induced Phase Separation: Effect of process parameters and development of an environmentally improved route assisted by supercritical carbon dioxide

S. Gay[a], G. Lefebvre[a], M. Bonnin[a], B. Nottelet[b], F. Boury[c], A. Gibaud[d], B. Calvignac[a,*]

[a] Micro & Nanomédecines Translationelles-MINT, UNIV Angers, INSERM U1066, CNRS UMR 6021, Angers F-49933, France
[b] Institut des Biomolécules Max Mousseron (IBMM) UMR 5247 CNRS-Université Montpellier-ENSCM, Faculté de Pharmacie, 15, Avenue Charles Flahault BP14491 34093 Montpellier Cedex 5, France
[c] CRCINA, INSERM, Université de Nantes, Université d'Angers, Angers, France
[d] Institut des Molécules et Matériaux du Mans, UMR-CNRS 6283, Université du Maine, 72085 Le Mans, France

GRAPHICAL ABSTRACT

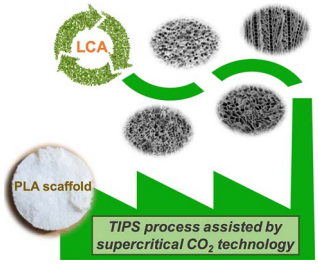

Keywords:
Scaffold
Polylactic acid (PLA)
TIPS
Supercritical CO_2
Life cycle assessment (LCA)

ABSTRACT

In this work, a relatively large scale of PLA scaffolds was produced using thermally induced phase separation (TIPS) combined with a supercritical carbon dioxide (SC-CO_2) drying step as a green alternative. For the TIPS step, the phase separation of PLA and 1,4-dioxane solvent was controlled by adjusting the process conditions such as the polymer concentration and molecular weight, the 1,4-dioxane solvent power and the cooling conditions. The scaffolds morphology was analyzed by scanning electron microscopy. Their structural and mechanical properties were correlated together with the possibility to tune them by controlling the process conditions. An environmental analysis using the Life Cycle Assessment (LCA) methodology confirmed a reduction of at least 50% of the environmental impact of the whole process using the SC-CO_2 drying compared to the traditional freeze-drying technology. This work is the first known attempt to conduct the LCA methodology on TIPS process for the PLA scaffolds production.

1. Introduction

Polylactic acid (PLA) is a biodegradable aliphatic polyester derived from renewable resources like corn starch. Since more than twenty years, bio-based polymers, particularly PLA, are increasingly investigated for scaffolds production [1–4]. A scaffold is a concept of substitute material for tissue engineering applications like bone and cartilage regeneration [5]. A scaffold must meet some requirements such as (i) a three-dimensional porous structure inside and on its surface to permit the transport of nutrients and cell adhesion, proliferation,

* Corresponding author at: Laboratoire MINT UMR INSERM U1066/CNRS 6021 IBS – CHU Angers, 4 rue Larrey, 49933, Angers CEDEX 9, France.
E-mail address: brice.calvignac@univ-angers.fr (B. Calvignac).

and differentiation to form a mimetic host tissue and to involve its regeneration [6], (ii) the biocompatibility because of the material degradability over time [7], (iii) the sufficient mechanical properties until the complete regeneration and reconstruction of the tissue [8], (iv) the easy and sustainable manufacturing process for shaping the material [9].

Many techniques have been developed for the production of this kind of materials, such as supercritical CO_2 (SC-CO_2) assisted processes [10], porogen leaching [11,12], emulsion freeze drying [13,14], 3D printing [15], gas foaming [16–18], Thermally Induced Phase Separation (TIPS) [19,20] and any possible combination of two of these techniques [1,21]. Among all these techniques, the ease of implementation due to the absence of required specific equipment makes TIPS one of the most effective processes to produce scaffolds with tunable properties [22]. It shows a good control of the scaffold structure, particularly porosity, pores diameter and interconnectivity [20], which play a significant and very often limiting role in tissue regeneration [23]. Indeed, these scaffold characteristics have an effect on different cell processes like adhesion, migration, proliferation and differentiation [24]. Besides, other scaffold properties can be controlled by TIPS such as mechanical properties [19] and biodegradability [25]. Basically, TIPS process is based on the principle that a homogeneous solution of a polymer dissolved in a good solvent can undergo a phase separation by cooling and can consequently cause the solution saturation which leads to polymer precipitation, followed by polymer structuration as a microcellular foam. The adjustment of the thermodynamic parameters, e.g. polymer concentration, cooling temperature or cooling rate, enables to promote one specific way of phase separation. As a function of polymer-solvent affinity, the TIPS process can follow two typical mechanisms (Fig. 1).

In case of a good compatibility of the polymer-solvent couple, such as PLA with 1,4-dioxane (Hansen Solubilty Parameters (HSP) respectively of 21.9 $MPa^{1/2}$ and of 20.5 $MPa^{1/2}$) [26], combined to a quite high freezing temperature of the solvent, Solid-Liquid (S-L) phase separation may occur (Fig. 1.a). The crystallization of the solvent part governs the structuration of scaffolds [27]. On the contrary a Liquid–Liquid (L-L) phase separation occurs under cooling when the polymer-solvent affinity is too weak. In this way, Schugens et al. [28] and Nam and Park [29] showed that the addition of water to a PLA/1,4-dioxane system can change the phase separation mechanism under cooling. The addition of water as a poor solvent of PLA (water HSP = 47.8 $Mpa^{1/2}$) lowers interactions between the polymer and the good solvent. Therefore, a liquid–liquid demixing occurs at higher temperature than the solvent freezing temperature. Typical diagram of L–L phase separation for polymer solution such as Upper Critical Solution Temperature (UCST) is introduced in Fig. 1b. According to the thermodynamic pathway (composition, temperature, time), the phase separation can show different behaviors [29,30]. Three scenarios can occur: the first one is a demixing that takes place below the binodal curve into the metastable region. The two phases separate following nucleation and growth mechanisms. This kind of separation provides a polymeric matrix with spherical or pseudo-spherical pores poorly interconnected. The second one, called spinodal decomposition, takes place when the spinodal curve is crossed with the formation of a 3D polymer network. The third scenario, mostly encountered, is a combination of the two previous mechanisms by crossing both curves. After the phase separation, when the temperature is smaller than the solution glass transition temperature, this one is frozen in a solid state composed of two solid phases, one rich in polymer and one rich in solvent.

After the phase separation, the obtained structure is frozen. The next step is to remove the solvent part to obtain the polymer scaffold. Traditionally this last step is carried out by freeze-drying. Freeze-drying can last between 3 days [14,29,30] and 1 week [31,32] and is particularly high energy-consuming. To reduce the duration and environmental cost of the whole process, SC-CO_2 drying technology seems to be an excellent alternative but rather scarcely studied until now [33]. Indeed, its good extraction properties reduce the processing time and the energy consumption. Furthermore Reverchon et al. [34] showed that SC-CO_2 extraction of 1,4-dioxane in PLA matrices could reduce the residual solvent below 263 ppm after 4 h, which is respectful of the 1,4-dioxane concentration limits (380 ppm) authorized by the Pharmacopeial convention. One major challenge of this study is also to guarantee the production of eco-friendly and safe materials, respectful of limits for residual solvents. Indeed, minimizing the energy consumption and environmental impacts is an important issue for industrial processes. Most of environmental impacts are fixed during the conception phase [35] thus, to be efficient, the implementation of an eco-friendly methodology has to be integrated as soon as possible during the process development. Life cycle assessment (LCA) was chosen in this work to compare objectively the two drying technologies during the whole process. LCA has already been used to compare the environmental costs of the production and use of PLAs with petrochemicals equivalent [36–38]. LCA literature is particularly well described for packaging [39–41] and building materials [42–44]. These two sectors are large consumers of polymer foams; nevertheless, no study concerning the production of PLA foams has been done.

The present paper aims at showing the potential of a more sustainable TIPS process assisted by the SC-CO_2 drying technology for the production of PLA scaffolds with tunable structural and mechanical properties. To go further in the process parametric study of this work,

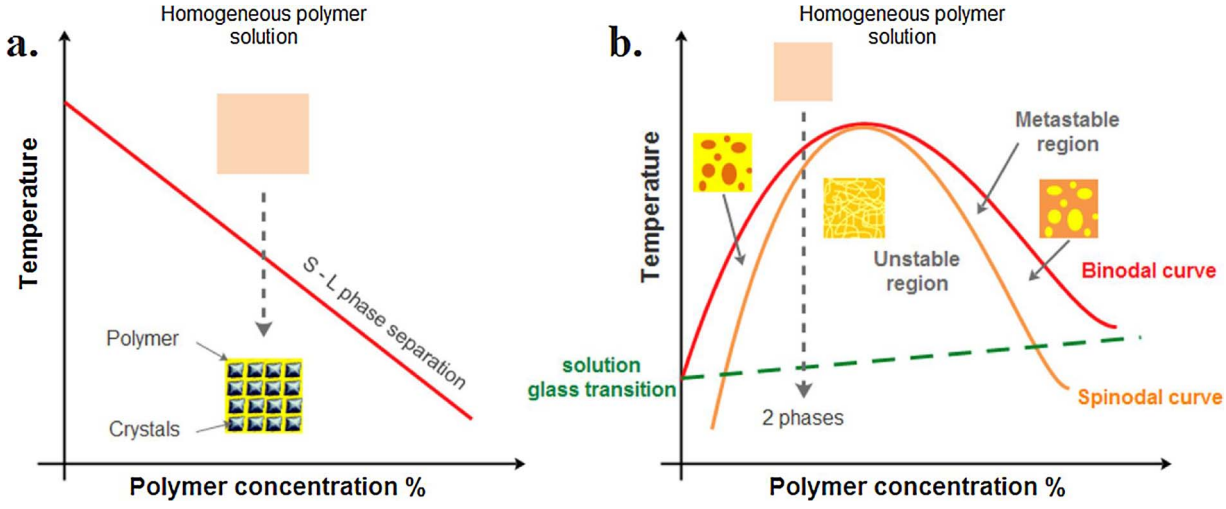

Fig 1. Thermally induced phase separation in polymer solutions: a) Solid-Liquid phase separation, b) Liquid–Liquid phase separation.

an environmental analysis of the process and its alternative cooling and drying technologies has been performed.

2. Materials and methods

2.1. Materials

PolyLactic Acid (PLA) was synthetized by the method described by Sardo et al. [45] and characterized by the methods described below. The PLA used in this study contains more than 99% of L-isomer, making it particularly crystalline, and is thus called PLLA. In preliminary experiments (not shown in this study), this PLLA showed a better ability to maintain the integrity of the scaffolds structure. 1,4-dioxane (ACS reagent > 99%) was bought from Sigma–Aldrich and its melting temperature is 12 °C. CO_2 (99.995 wt%, Linde, Germany) was used as the drying agent. To date, no green alternative solvent has shown the same properties as 1,4-dioxane, i.e. a high freezing temperature solvent with a high affinity with PLLA.

2.2. Polymer characterization

The number average molecular weight (Mn), the weight average molecular weight (Mw) and the dispersity (ð) of the polymers were determined by size exclusion chromatography (SEC) using a Viscotek GPCMax autosampler system fitted two Viscotek LT5000L mixed medium columns (300 × 7.8 mm), a Viscotek VE 3580 RI detector. The mobile phase was THF at 1 mL/min flow and 30 °C. Typically, the polymer (20 mg) was dissolved in THF (2 mL), and the resulting solution was filtered through a 0.45-µm Millipore filter before its injection (20 µL). Mn was expressed according to calibration using polystyrene standards. The Mn values were also determined by ^{1}H NMR. ^{1}H NMR spectra were recorded at room temperature using an AMX300 Bruker spectrometer operating at 300 MHz. Deuterated chloroform was used as a solvent, chemical shifts were expressed in ppm with respect to tetramethylsilane (TMS).

2.3. Scaffolds formulation

The method described below enables to produce 50 scaffolds in one batch to demonstrate the scale-up potentiality of this process. Fig. 2 illustrates the different steps of the process.

Firstly, PLLA/1,4-dioxane solutions were prepared by dissolution of polymer in the solvent under 500 rpm stirring at 50 °C. The amount of PLLA was comprised between 5 wt% and 10 wt% to obtain high porous scaffolds. For L–L phase separation process, water was added after complete dissolution of the polymer in the 1,4-dioxane. A volume of 1 mL of the obtained solution was poured in cylindrical aluminum molds of 12 mm diameter. The duration of this step was minimized to avoid any phase separation before the cooling operation. For the phase separation, three cooling conditions were applied by putting the samples in a cold storage at −20 °C or −80 °C, or by soaking them in liquid nitrogen (–196 °C). The choice of these cooling temperatures was done in order to impose different cooling rates and consequently different crystallization conditions. To ensure the complete stabilization of the temperature, samples were left 12 h in the cold storages and at least 5 min in liquid nitrogen. When samples were frozen, they were extracted from the aluminum molds and immersed in 10 mL of pre-cooled ethanol at −20 °C to extract the 1,4-dioxane during at least 2 h in a cold storage (4 °C). This step was necessary to extract the solvents mixture with SC−CO_2. Finally, 50 samples were placed in a stainless autoclave with a capacity of 500 mL (Separex, Champigneulles, France) heated at 35.0 ± 0.1 °C and pressurized with CO_2 at 150 ± 1 bar. Liquid CO_2 at 4 °C was continuously pumped at a rate of 1 ± 0.1 kgh^{-1} by a high-pressure membrane pump (Milton Roy Europe, Pont Saint Pierre, France) and was preheated by a heat exchanger (Separex, Champigneulles, France) before feeding the autoclave. The autoclave pressure was kept constant by means of a back-pressure regulator (Swagelok, Solon, USA) during 4 h for solvent extraction, and then the autoclave was slowly depressurized at 2.5 barmin^{-1} to avoid any deformation of the samples.

2.4. Differential scanning calorimetry (DSC) measurements

Thermal properties and crystallinity of PLLA and scaffolds were evaluated by DSC. Measurements were carried out under nitrogen on a Perkin Elmer Instrument DSC 6000 Thermal Analyzer. Samples were submitted to the following treatment: *(i)* Heat from 20 °C to 200 °C at 5 °C min^{-1} ($Tm_1/\Delta Hm_1$; $Tc_1/\Delta Hc_1$; Tg_1), *(ii)* Hold for 10 min at 200 °C, *(iii)* Cool from 200 °C to −10 °C at 5 °C min^{-1} ($Tc_2/\Delta Hc_2$), *(iv)* Hold for 10 min at −10 °C, *(v)* Heat from −10 °C to 200 °C at 5 °C min^{-1} ($Tm_2/\Delta Hm_2$; Tg_2). The crystallinity rates of polymers and scaffolds were calculated by the following formula $Xc = \Delta Hm1/\Delta Hm_{PLA}$ with $\Delta Hm_{PLA} = 91 \pm 3\ J\ g^{-1}$ [46].

2.5. Phase diagram determination

Binary solutions were studied by crystallization temperature measurements whereas ternary solutions were studied by cloud point measurements. The crystallization and cloud point were determined visually by turbidimetric measurements, following Hua et al. procedure [47]. The different mixtures were prepared under stirring at 600 rpm at 60 °C until the complete dissolution of PLLA in 1,4-dioxane, then if needed water was added under 600 rpm stirring during 15 min. Afterwards, all the mixtures held in closed vials were placed in a water bath at 60 °C. The temperature was then slowly decreased by steps of 1 °C every 10 min. The temperature at which the mixtures changed from clear to cloudy corresponded to the crystallization point or to the cloud point, respectively for the binary or ternary solutions. The precision of

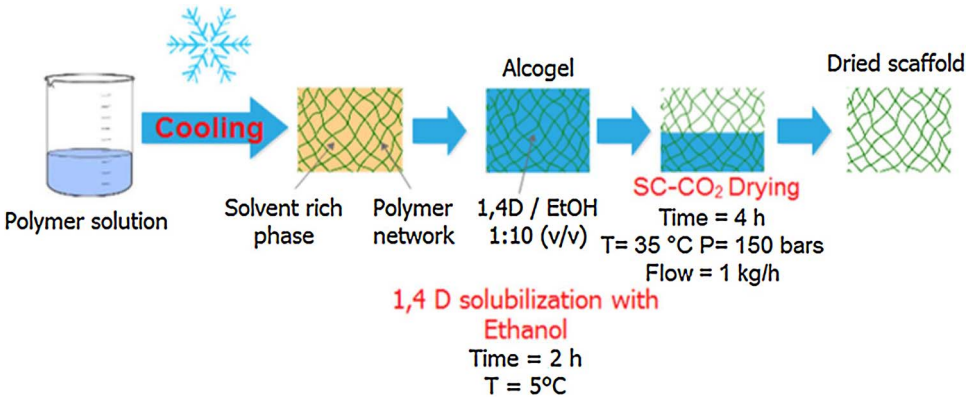

Fig. 2. Scheme of the TIPS process coupled with SC-CO_2 drying.

Table 1
Goal and scope of LCA.

Functional unit	Production of 50 units of PLA scaffolds of 1 mL each
System boundaries	From resource extraction to scaffolds production: management of scaffolds as waste has not been considered
Assumption and limitation	No impacts have been considered for the building where the experiment have been performed or for the "big materials" (cold storage, etc.) as it has been assumed that their impacts are negligible regarding their lifetime
Allocation method	The "default system" allocation method proposed in Ecoinvent v3.0 database, based on economic or physical flows, has been retained
Impact categories	The 18 impact categories of the ReCiPe v1.10 method have been conserved

the visually observed measurements was about 1 °C.

2.6. Scanning electron microscopy (SEM) and pictures analysis

Scaffolds morphology was observed by SEM on a JEOL 6301F (JEOL Paris, France). A thin layer was cut in the centre of the scaffolds. This sample was coated with a thin layer of platinum by sputtering with a high vacuum coater (Leica EM ECA600, Leica, France). Images were captured at a 3 kV acceleration voltage in the secondary electron mode and a working distance of 20 mm.

The pore size and cell density of scaffolds were determined by image analysis using imageJ [48] freeware on the SEM micrographs. The pore size distributions were obtained by measuring at least 30 pores by picture. Due to the pores anisotropy, the smallest diameter has been retained for pore size measurements. The cell densities were obtained by counting the number of pores in scaled area. For one sample, three regions were measured.

2.7. Bulk density measurements

The bulk density ρ of scaffolds was assessed by water displacement method. The whole sample was firstly weighted dry, and secondly weighted in a 25 mL measuring cylinder filled with water. Because of the buoyancy of the scaffolds, a metal cylinder with a known volume was used to maintain the scaffold at the bottom of the measuring cylinder. In this method, it was assumed that the water did not penetrate within the sample because of the small size of external pores and the short time of immersion. This method also enabled to calculate a global porosity ε of our samples from the following equation:

$$\varepsilon(\%) = \left(1 - \frac{\rho_{\text{scaffold}}}{\rho_{\text{poylmer}}}\right).100$$

2.8. Mechanical tests

The compressive properties of the scaffolds including compressive strength and compressive modulus were measured with an ADAMEL LHOMARGY DY 34 B tension/compression machine with 1 kn sensor (Adamel Lhomargy, Roissy-en-Brie, France). Each circular specimen of 11 mm of diameter and 5 mm of thickness was compressed at a compression rate of 1 mm min^{-1}. The compressive modulus, yield stress and yield strain were obtained by averaging three measurements made on three different samples.

2.9. Life cycle analysis (LCA)

Environmental assessment of processes can be performed thanks to many different methods: qualitative or quantitative approach, mono or multicriteria analysis, on the all life cycle or on specific steps, etc. It has been decided here to adopt the LCA method, which is a very comprehensive approach used for assessing all the environmental impacts of a process or product "from cradle to grave", which means from the resource extraction to the waste management. Different tools and calculating methods exist to implement this method. The widely used SimaPro® software v8.0.3 has been selected for the model simulation, together with the impact calculation method ReCiPe v1.10 (http://www.lcia-recipe.net) midpoint impact categories (H) and the database Ecoinvent v3.01 (http://www.ecoinvent.org/). The LCA methodology has been defined in the standard ISO 14040 [49], following four steps. The first step was to define precisely the goal and scope of the study. This means to define the functional unit and the system boundaries, to highlight any assumption and limitation and to choose an allocation method and the impact categories retained. The objective here was to compare the environmental impacts of the different alternatives previously detailed for the production of PLA scaffolds. The management of PLA scaffolds once a waste was not considered here, thus the LCA was simplified as a "cradle to gate" approach. Table 1 details the goal and scope of this study.

In a second step (Life Cycle Inventory analysis), all mass and energy flows within the system boundary were inventoried referring to the functional unit. Then, in a third step (Life Cycle Impact Assessment), the environmental impacts of these mass and energy flows were assessed. In the last step, all results were summed up and interpreted to derive potential improvements or to support decisions between different options.

3. Results and discussion

3.1. Polymer characterization

Two different molecular weights of the PLLA were synthetized. Their number average molecular weight (Mn), weight average molecular weight (Mw), dispersity (ð) and crystallinity are introduced in Table 2.

From now on, these two polymers will be respectively called PLLA 96 and PLLA 162, on the basis of their Mw values.

3.2. Phase equilibria of PLLA/1,4-dioxane and PLLA/1,4-dioxane/water systems

The SC-CO_2 drying step performed with our operational conditions is not known to modify PLA scaffolds structure, either by deformation [50] or by foaming [51]. Thus, considering that the phase separation governed the final structure of the material, the control of this step was the major challenge of TIPS process. In a solution composed only of PLLA at low concentration in 1,4-dioxane, the phase separation was a solid-liquid (S-L) type. In this case, the foam shaping was caused by the 1,4-dioxane crystallization. Fig. 3a shows the crystallization temperature of binary solutions of PLLA 96 and PLLA 162 at different concentrations. With a crystallization point of 4 ± 1 °C for the pure 1,4-dioxane solvent, the effect of polymer concentration and molecular weight could be considered as negligible with a crystallization point

Table 2
Molecular weight, dispersity and cristallinity of the two PLLA.

Designation	Mn RMN (kDa)	Mn SEC (kDa)	Mw SEC (kDa)	ð	Crystallinity (%)
PLLA 162	96 350	101 000	162.6	1.61	66
PLLA 96	69 050	60 000	96	1.60	60

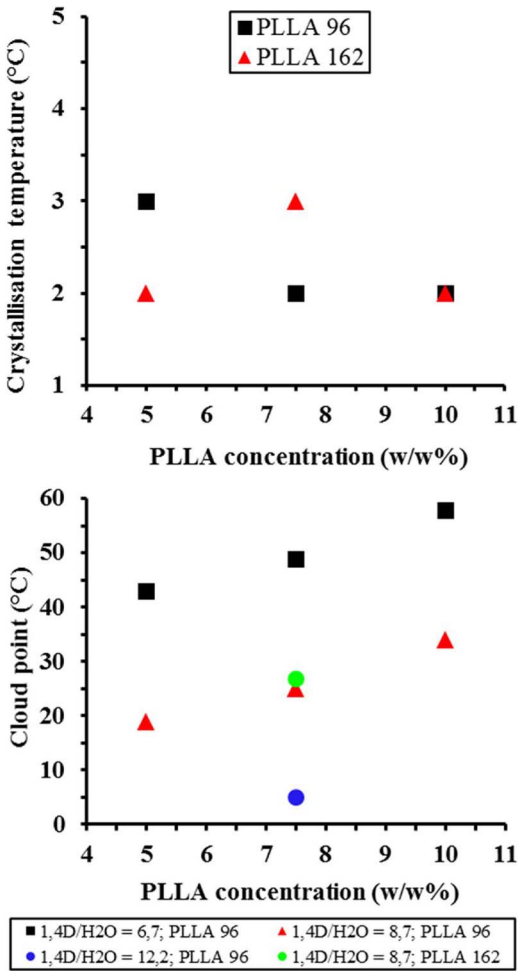

Fig. 3. S-L phase equilibrium (a) and L–L phase equilibrium (b) of PLLA/1,4-dioxane and PLLA/1,4-dioxane/water systems, respectively.

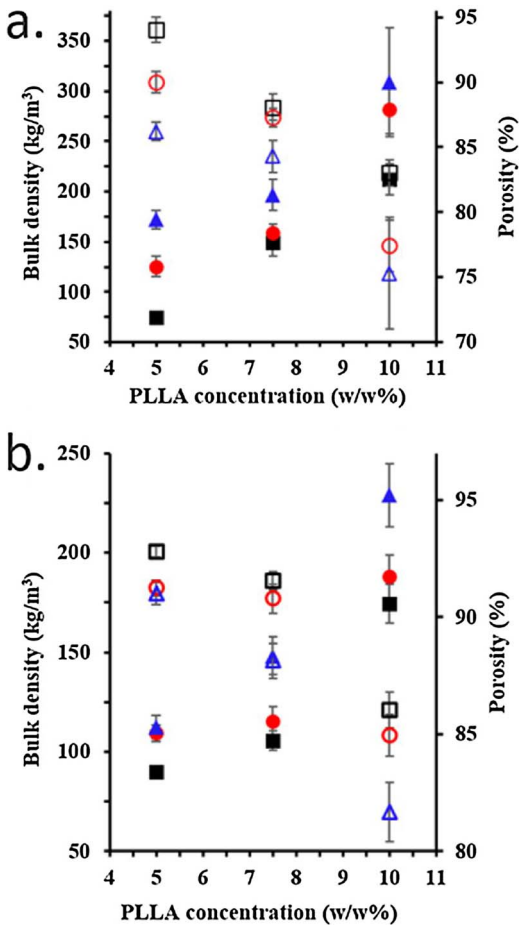

Fig. 4. Evolution of scaffolds density with the PLLA concentration from (a) S-L phase separation (PLLA 96) and (b) L–L phase separation (PLLA 96; 1,4-dioxane/H_20 = 8.7). Filled symbols and open symbols refer to bulk density and porosity, respectively. Black squares, red circles and blue triangles refer to −20 °C, −80 °C and −196 °C, respectively. (For interpretation of the references to colour in this figure legend, the reader is referred to the web version of this article.)

between 2 ± 1 °C and 3 ± 1 °C for all the binary solutions with polymer concentrations between 5% and 10%. These measurements and observations were in good agreement with Schugens et al. [28] results for PLLA polymers with higher molecular weight.

In ternary mixtures, L–L phase separation was promoted due to the addition of water as a poor solvent of PLLA but miscible in 1,4-dioxane. The cloud point measurement was a simple way to evaluate the L–L phase separation temperature. Fig. 3b shows the effect of three different 1,4-dioxane/H_2O ratios (6.7, 8.7 and 12.2) for one weight average molecular weight of 96 kDa of the polymer (PLLA 96) and the effect of two different molecular weights (96 and 162 kDa) for a 1,4-dioxane/H2*O* ratio of 8.7. The graph shows that at fixed PLLA content, the cloud point temperature of the solution increased with the water content. Moreover, it highlights that the cloud point temperature increased with the polymer concentration. This result has been previously observed by Hua et al. [52]. Besides, a slight increase of the cloud point from 25 °C to 27 °C with the molecular weight has been measured. According to the literature, the polymer dissolution rate decreased with the molecular weight [53]. Regardless of the mechanism of phase separation, S-L or L-L, the results obtained respectively with binary PLLA/1,4-dioxane and ternary PLLA/1,4-dioxane/water mixtures showed that the temperature of phase separation should impact the final material.

3.3. Structural properties of PLLA scaffolds

The bulk density is often a selective criterion to characterize a porous material because it is linked to its mechanical properties. As expected, the bulk density of scaffolds was increased with the polymer concentration (Fig. 4). Moreover, the density increased when the cooling temperature decreased. This result could be due to a faster cooling rate which involved a freezing point depression of the polymer solution. These bulk density values between 75 and 310 kg m^{-3} were correlated with porosity values between 75 and 94%, which are classically found in tissue engineering applications [54,55].

The internal pore structures were observed by SEM. Fig. 5 shows different scaffold morphologies obtained with binary solutions from 5 wt% to 10 wt% of PLLA at three different cooling temperatures. All observed scaffolds had anisotropic pores close to a parallelepiped shape. From these observations, shapes and organizations of scaffold pores were assumed to be due to the 1,4-dioxane crystallization and the influence of temperature gradient. Indeed, this gradient seemed to induce the orientation of the structure in a preferential direction. The orientation was more pronounced at cooling temperature of −80 °C and −196 °C than at −20 °C because of the higher induced gradient between the walls and the heart of the sample. It is a well-known effect [56] used to orientate the structure of PLLA membranes produced by the TIPS process.

It is also clear in Fig. 5 that the cell density increased with a strong cooling. Indeed, at −20 °C, −80 °C and −196 °C, maximum pore sizes are respectively ranging from 15 to 55 µm, from 5 to 40 µm and from 1 to 10 µm, depending on the PLLA concentration (Fig. 6).

Regarding tissue engineering applications, the optimal pore size also varies for different cell types, with pore sizes ranging from 50 to 70 µm

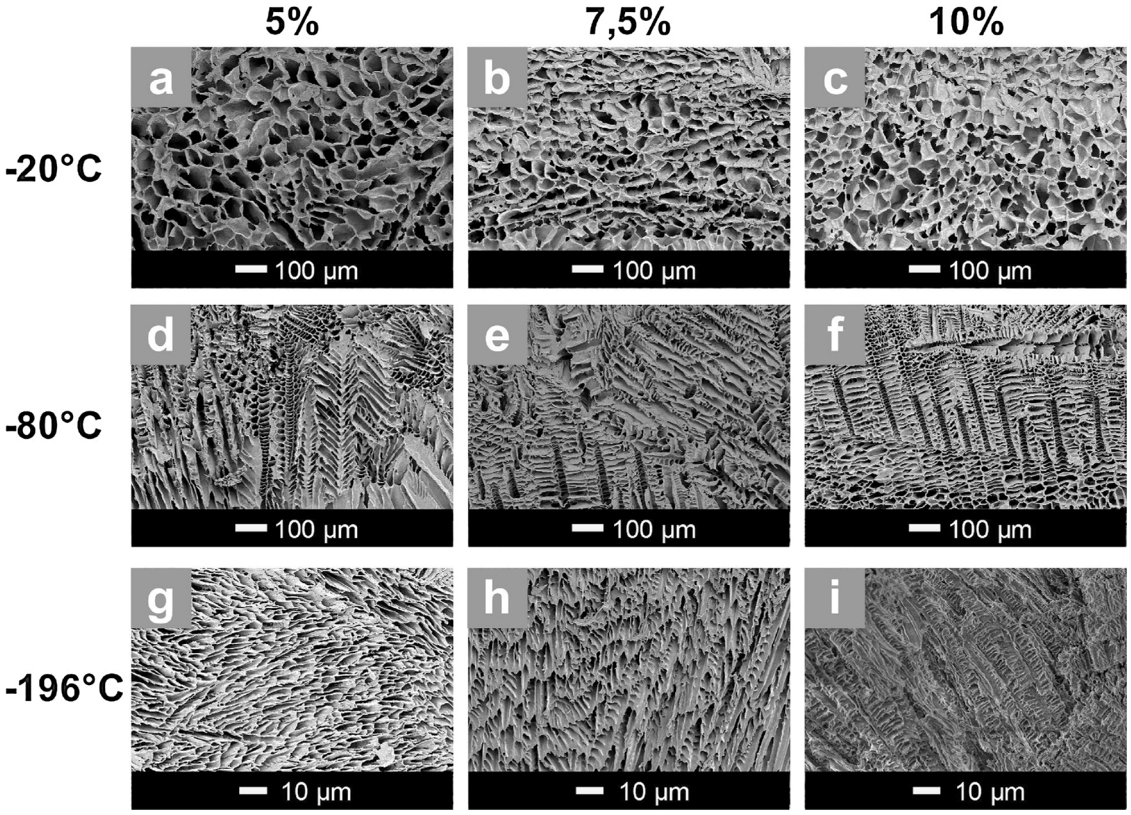

Fig. 5. SEM pictures of scaffold structures obtained with binary solutions of PLLA 96 and 1,4-dioxane for various polymer concentrations and cooling temperatures (please note that magnifications change at −196 °C to be able to see the structure).

suitable for microvascular and cardiac cells [57], 75–200 μm suitable for nutrient diffusion and circulation of growth factors in trabecular bone [55], 50–160 μm for fibroblasts [58] and nerve cells [59], and close to 20 µm for hepatocytes [60]. This effect of the cooling temperature, and thus of the cooling rate, on the pore size has already been observed by Schugens [27]. When the cooling temperature was getting closer to the crystallization temperature of the solution, the growth of large crystals was favoured. On the contrary, when the cooling temperature was far from the crystallization temperature of the solvent, the nucleation was favoured. These observations have been confirmed by the cell density calculation, which allowed to get rid of the anisotropy. Values were obtained by counting the pores on a known area on SEM pictures: results are introduced in Fig. 7. Scaffolds produced at −20 °C, −80 °C and −196 °C showed a cell density between 200 n mm^{-2} and 500 n mm^{-2}, between 1000 and 3500 n mm^{-2} and between 5800 n mm^{-2} and 56000 n mm^{-2}, respectively.

Fig. 7 also attests that cell density (calculated from SEM observations) increased with PLLA concentration. This was due to the fact that additional material constrained crystal growth and consequently increased the number of small crystals. As already observed [27], no significant effects of PLLA molecular weight on the scaffold morphologies have been noticed (results not shown). This proved that the supposed increase of viscosity due to a higher molecular weight did not affect the 1,4-dioxane crystallite formation. All these results confirmed that the control of the crystallization, especially by the temperature, is the key parameter of the scaffold production by S-L phase separation.

In ternary solutions, the thermodynamic pathway and the kinetics impacted the obtained structure of PLLA scaffolds. Indeed, kinetics were directly governed by the cooling temperature. However, in this work, all scaffolds obtained by L–L phase separation led to relative isotropic structures. Fig. 8 shows the effects of the cooling conditions and PLLA concentrations (for 1,4-dioxane/water ratio about 8.7) on the scaffolds structure.

Fig. 9 shows the effect of water content on scaffolds structure obtained with fixed PLLA content (7.5 wt%) and cooling condition (–20 °C).

All structures obtained at −20 °C (Figs. 8a–c and 9) were composed of nanofibers assembled together. Liu et al. reported that nanofibers structure was related to the L–L phase separation and subsequent nucleation and crystallization growth in the polymer-rich phase [61]. Besides, similar structures to Figs. 8a and 9 have been observed by Zhang et al. [62] in thermal phase separation of PLLA/DMF solutions. The obtained structures seemed to form micro-sheaves around few micrometers, attributed to a radially crystal growth of PLLA. At lower cooling temperatures at −80 °C (Fig. 8d–f) and at −196 °C (Fig. 8g–i) PLLA fibrous structure disappeared in favour of a denser network confirmed by the density measurements (Fig. 4b). It seemed that when the cooling was too slow, a self-arrangement of PLLA molecular chains may occur in a more favourable thermodynamically state. This led to poorly cohesive materials.

On the other hand, scaffolds obtained at lower temperature seemed to show a more cohesive structure. The interconnected network shown in Fig. 8d and g seemed to reveal that the solution solidified in the unstable region. Meanwhile, spherical pores observed in Fig. 8e and f seemed to result from a metastable region. Finally, Fig. 8d and g show that a PLLA concentration about 5 wt% and cooling temperature below −80 °C favoured the formation of open structures with a connection to the outside of the scaffold's surface. Regarding tissue engineering applications, the fibrous PLLA scaffolds would enable to improve protein adsorption for cell attachment [63] like osteoblasts, which would proliferate more effectively on rough surface. Besides, cell migration through the scaffold surface would be possible with pore size above 3 µm [64].

Another key parameter of L–L phase separation is the water content and consequently the Hansen solubility parameter of the solvent part (Fig. 9). At low water content, scaffolds were composed of micro straw-

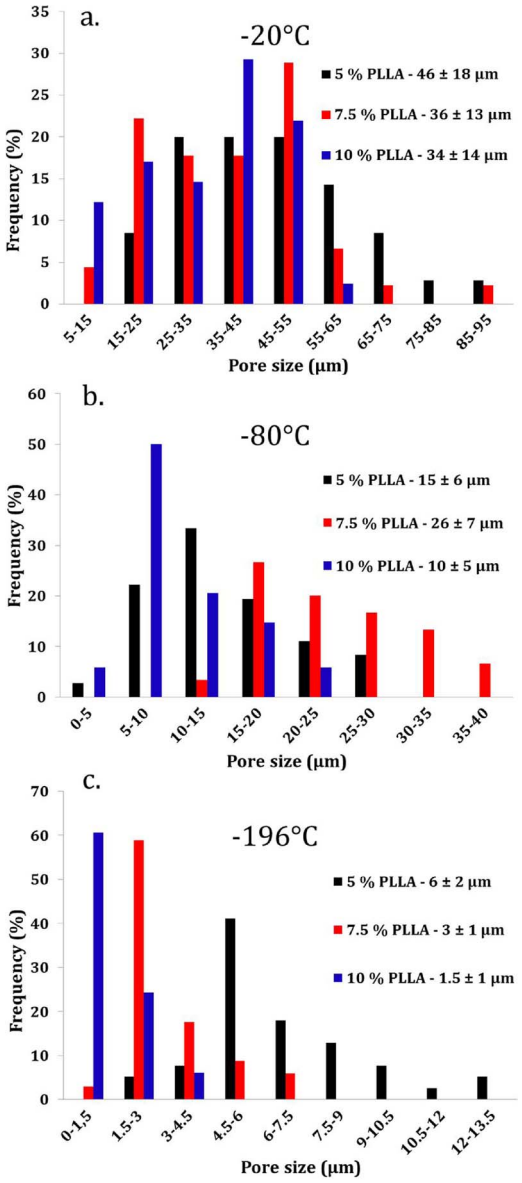

Fig. 6. Pore size of scaffolds obtained with binary solutions of PLLA 96 and 1,4-dioxane for three polymer concentrations and three cooling temperatures. Average pore sizes and standard deviations are specified in the figure captions for each condition.

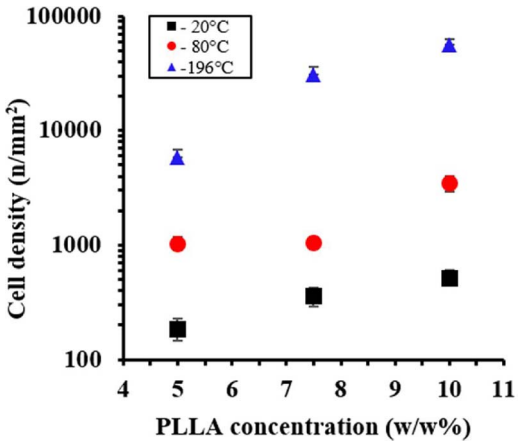

Fig. 7. Evolution of cell density of PLLA 96 scaffolds with concentration for various cooling conditions of binary solutions PLLA/1,4-dioxane.

sheaf structures (Fig. 9a), whereas when the water content increased, scaffolds were composed of spherical pores with size up to 100 µm (Fig. 9c). This spherical structure was characteristic of binodal phase separation which was due to an important reduction of interactions between the solvent and polymer. The increase of the water content seemed to confine the PLLA chains and consequently prevented the preferential rearrangement. This could explain why the structure obtained with higher water content looked tougher at the macroscopic scale as the mechanical tests confirmed.

Effects of temperature and water content have been already evaluated [29,30], but little is known about the effect of the PLLA molecular weight. Fig. 10 shows PLLA scaffolds with a weight average molecular weight of 96–162 kDa and at fixed composition of a ternary mixture PLLA/1,4-dioxane/H_2O.

The molecular weight increase induced a significant decrease of the pores diameter from 10 to 1 µm. It could be assumed that the length of the polymer chains limited their arrangement and/or the higher viscosity limited the coalescence of the solvent part. It was difficult to explain clearly this phenomenon, but it was obvious that an increase in molecular weight modified the structure of the obtained scaffold.

3.4. Mechanical properties of PLLA scaffolds

In the present work, compressive modulus, yield stress and yield strain were characterized by simple compressive tests. Ten series of samples were tested in triplicate to highlight the effects of process parameters, PLLAs molecular weight and scaffold morphologies on the mechanical properties. Characteristics of scaffold formulations are reported in Fig. 11. The values were extracted from stress-strain curves. The samples exhibited a well-described foam response under compression with the following three regions (*i*) linear elastic, (*ii*) a plastic plateau and (*iii*) densification [65].

The compressive modulus and the yield stress of PLLA scaffolds increased linearly with the polymer content (samples A, D and E of Fig. 11), whereas the yield strain decreased. It means that the increase of PLLA content, and consequently of density too, led to a more rigid material. This measured result confirmed previous results qualitatively observed [27]. For a fixed PLLA content, the compressive modulus decreased and the yield strain increased with the cooling temperature (samples B and C). These results were in contradiction with the increase of density previously measured. It could be only attributed to the morphology and probably to the decrease of pore size. Thus, the −20 °C temperature was the suitable cooling temperature to obtain scaffolds with an optimal, i.e. higher, Young modulus. This temperature was also the most sustainable cooling conditions (see the next part). In this way, this temperature was chosen to perform the production of the scaffolds D to I. Moreover, as it was previously observed in Fig. 5, these cooling conditions allowed to obtain scaffolds with the larger pore size (between 40–80 µm), which were suitable to facilitate cell seeding and migration, as well as the diffusion of the nutrients and oxygen throughout the whole structure [66]. Besides, a significant stiffening of scaffolds was found with the increase of molecular weight (samples A and F) although no difference in morphology has been noticed (Fig. S1). The crystallinity rate of samples A and F, evaluated by DSC, was respectively of 51% and 48%. This crystallinity difference is relatively low. Besides, a higher crystallinity rate of polymers should lead to stiffer materials [67–69]. This showed that the stiffness difference between the samples A and F was rather caused by the molecular weight difference. Thus, it would be possible to modulate the mechanical properties of the scaffolds by adjusting the molecular weight of the polymer.

The comparison of the samples E and F which had similar mechanical properties, implied that the scaffold production of F series would be more environmentally sustainable thanks to the PLLA savings up to 25% (polymer concentration about 10% for E and 7,5% for F) with higher molecular weight of PLLA (96 kDa for E and 162 kDa for F).

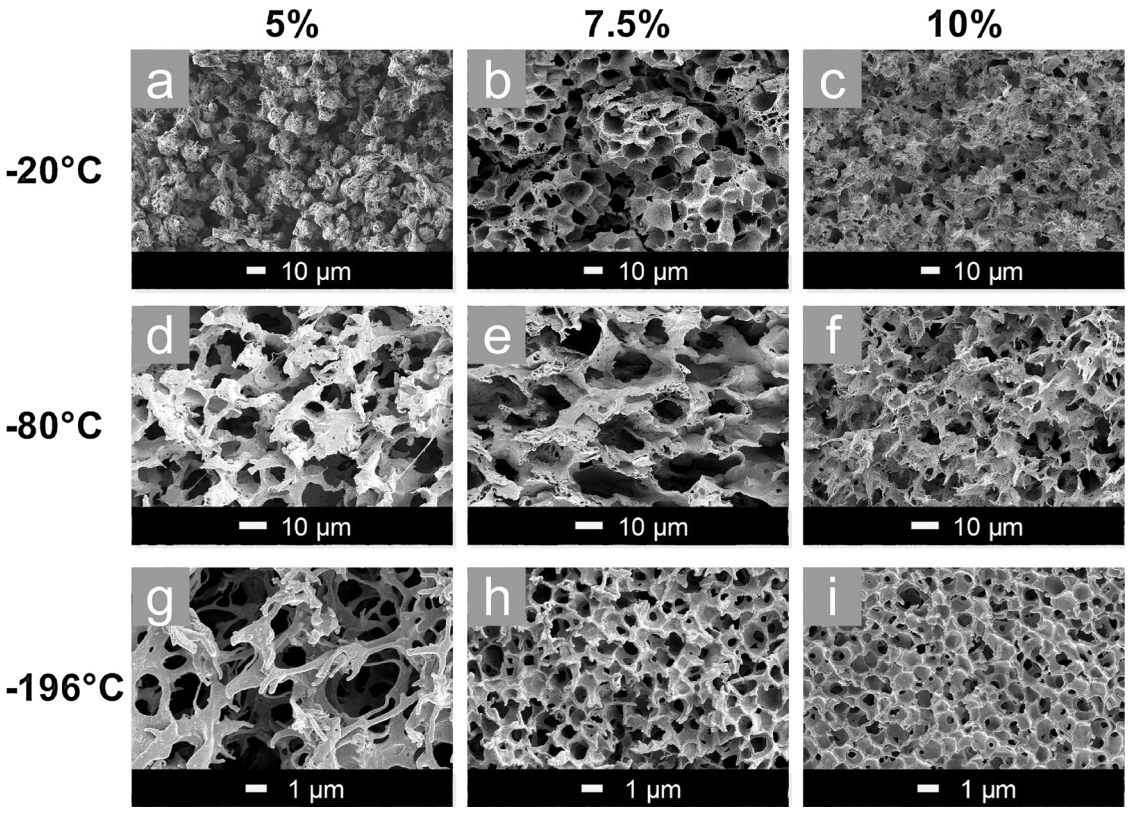

Fig. 8. SEM pictures of scaffold structures obtained from a ternary solution of PLLA 96/1,4-dioxane/H_2O with various PLLA concentrations (1,4-dioxane/$H_2$0 ratio = 8.7) and cooling temperatures (please note that magnifications change at −196 °C to be able to visually characterize the pores structure).

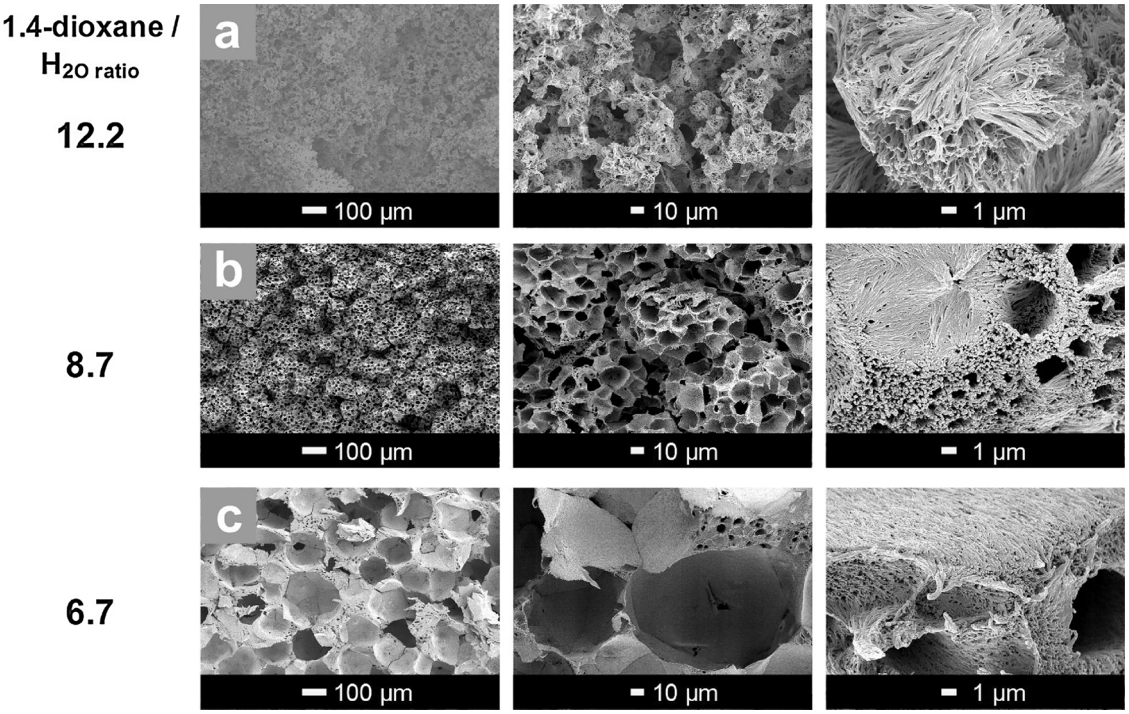

Fig. 9. SEM pictures of scaffold structures obtained at −20 °C from ternary solutions PLLA 96/1,4-dioxane/H_2O with a fixed PLLA content (7,5 wt%) and various weight ratios of 1,4-dioxane/H_2O.

Consequently, these optimal process conditions showed the possibility to obtain PLLA scaffolds from S-L phase separation with tunable microstructures and mechanical properties which could be relevant for the development of osteogenic scaffolds [5].

Scaffolds from samples G, H and I (Fig. 11) have been obtained from L–L phase separation. Both solutions G and H with higher 1,4-dioxane/H_2O weight ratios presented a poor strength. This weakness could be due to the poor cohesive structures observed in Fig. 9. However, the

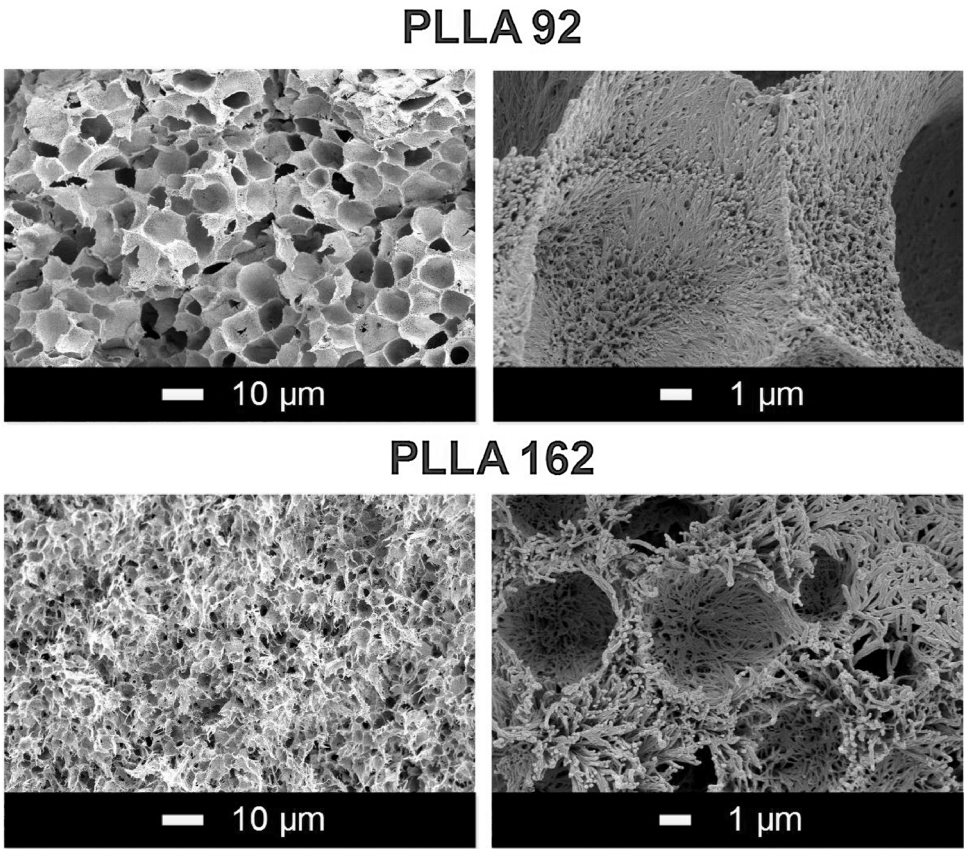

Fig. 10. SEM images of scaffold structures obtained from ternary solutions PLLA = 7.5% and 1,4-dioxane/H_2O ratio = 8.7 with PLLA 96 and PLLA 162.

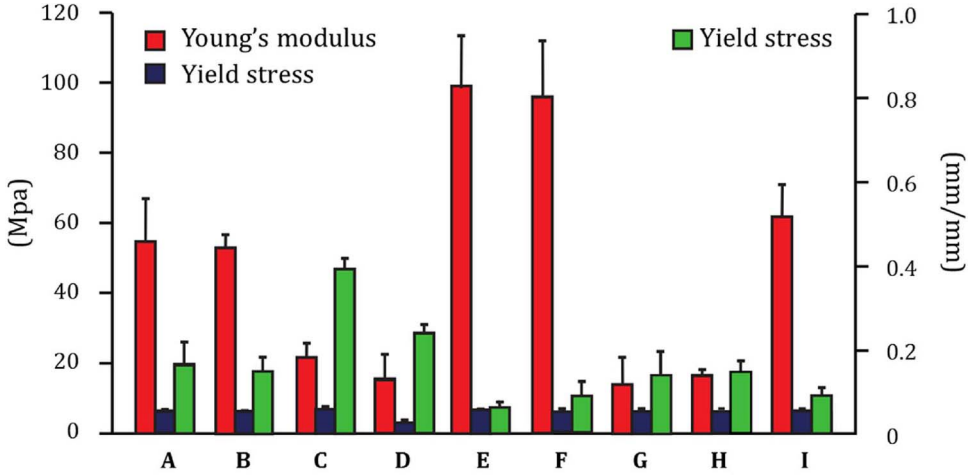

	A	B	C	D	E	F	G	H	I
Cooling temperature (°C)	**-20°C**	**-80°C**	**-196°C**	-20°C	-20°C	-20°C	-20°C	-20°C	-20°C
Polymer concentration (w%)	7.5	7.5	7.5	**5**	**10**	7.5	7.5	7.5	7.5
Molecular weight (kDa)	96	96	96	96	96	**162**	96	96	96
1,4D / H_2O ratio	/	/	/	/	/	/	**12.2**	**8.7**	**6.7**
Average Pore size ± SD (µm)	36 ± 13	26 ± 7	3 ± 1	46 ± 18	34 ± 14	45 ± 14	NC	9 ± 4	138 ± 40
Porosity (%)	88.1	87.3	84.2	94.0	83.0	88.0	91.0	91.6	91.3

Fig. 11. Effect of formulation parameters on the scaffolds mechanical properties. The table also includes the pore size and porosity results.

samples with the high-water-content, like the I series, showed a higher mechanical strength due to the spherical structure of scaffolds and the PLLA chain confinement involved by the binodal phase separation. These results were in good agreement with the SEM observations.

As a conclusion, the mechanical properties of the scaffolds obtained by S-L and L–L phase separations make them likely to be of interest for bone and cartilage regeneration application, for instance osteoporosis and osteoarthritis disorders. Indeed, the Young modulus values cover the range of values of cartilage (0.45–1 MPa) [70] and cancellous bone (40–460 MPa) [71,72]. Besides, in order to sublimate these potentialities and to enhance their biomimetic characteristics, the scaffolds may be modified by the blending of well controlled synthetic calcium carbonate particles ($CaCO_3$) obtained by our own developed supercritical carbonation process [73–79]. Indeed, calcium carbonate appears as an interesting candidate for tissue engineering applications because of the clinical use of $CaCO_3$ derived from natural corals as a bone graft substitute [80] or use in maxillofacial surgery [81]. Recently, Gandolfi et al. produced this kind of hybrid biomaterials for biomedical application [82].

3.5. Life cycle assessment (LCA)

The LCA conducted here aimed at comparing the environmental impacts of the different alternatives previously detailed for the production of PLLA scaffolds. Life cycle inventory involved the collection of all raw materials, energy and water flows that came inside the system boundaries, as well as all the outputs (emissions to air, water and soil) for each of the alternatives. All these data have been provided in Fig. 12.

Environmental impacts of these cooling conditions have been assessed and are reported in Fig. 13.

For both cold storages (−20 and −80 °C), electric consumptions were calculated from the original equipment manufacturer data and considering the volume occupied by 50 scaffolds. For −196 °C cooling scenario, 300 g of liquid nitrogen was necessary to freeze the scaffolds. Some precisions about all calculation and hypothesis have been listed in supplementary information (Table S1). As expected, the stronger the cooling, the higher the impact. As the parametric study showed that cooling conditions also influenced the scaffold structure and properties, this result was not to be used as a decisive criterion. Yet, it showed that

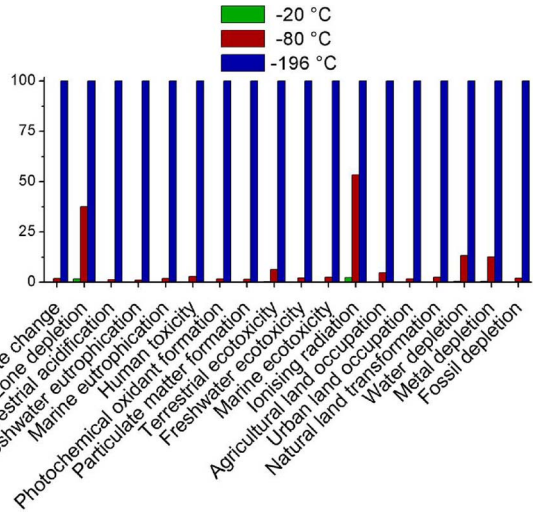

Fig. 13. Environmental impact assessment for the cooling conditions of the TIPS process (−20, −80 and 196 °C).

cooling at −196 °C with liquid nitrogen led to a high increase of all the LCA impacts compared to a cold storage at −80 °C. The most impacting cooling process (–196 °C) was selected for the simulation of the complete process to maximize the impact of this step and see its importance on the global life cycle.

Hence, the complete system has been modelled with the liquid nitrogen cooling process and the two drying alternatives: SC-CO_2 drying vs freeze-drying. As previously stated, the drying step should not affect the scaffolds structure because the structure was fixed at the cooling step. Therefore, the environmental impact of the whole process using either the SC-CO_2 drying or the freeze-drying could be compared. Fig. 14 shows clearly the benefits and reasons to choose the SC-CO_2 drying technology. Indeed, all environmental impacts were at least 50% reduced in comparison with the freeze-drying technology. Regarding freeze-drying, the high impact was particularly due to the important duration of the drying (96 h), estimated from previous studies [14,29,83] leading to a very high electricity consumption.

To better understand these results, a more detailed study has been

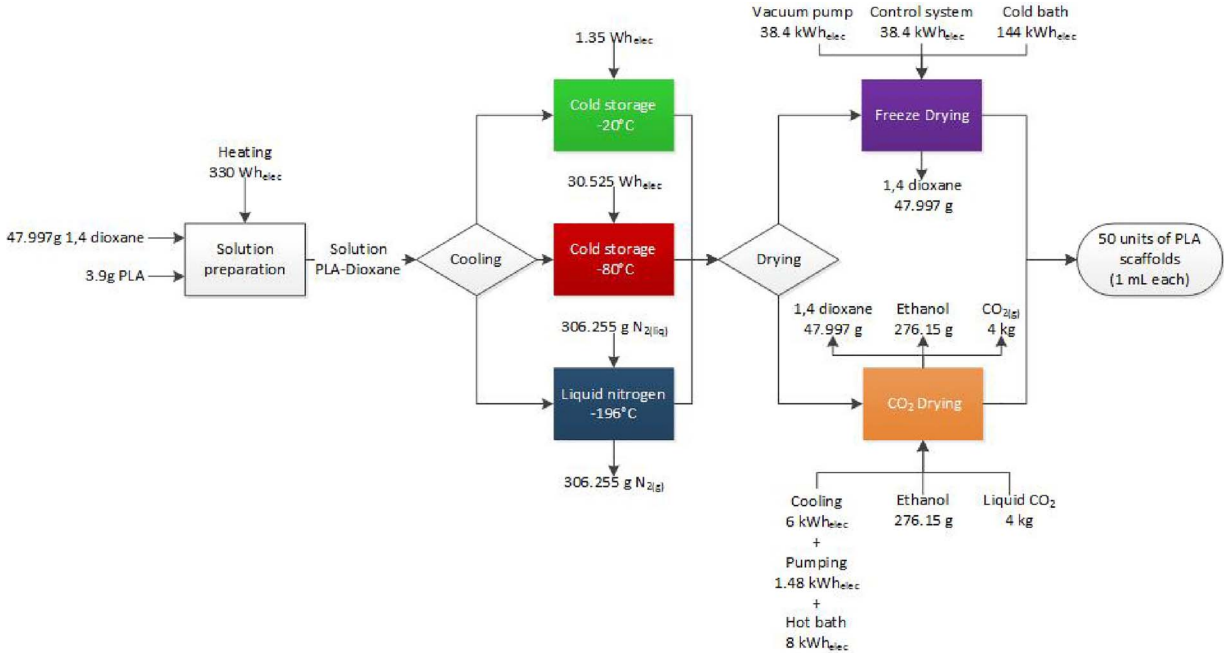

Fig. 12. Mass and energy balances for the production of 50 PLLA scaffolds according different cooling and drying scenarios.

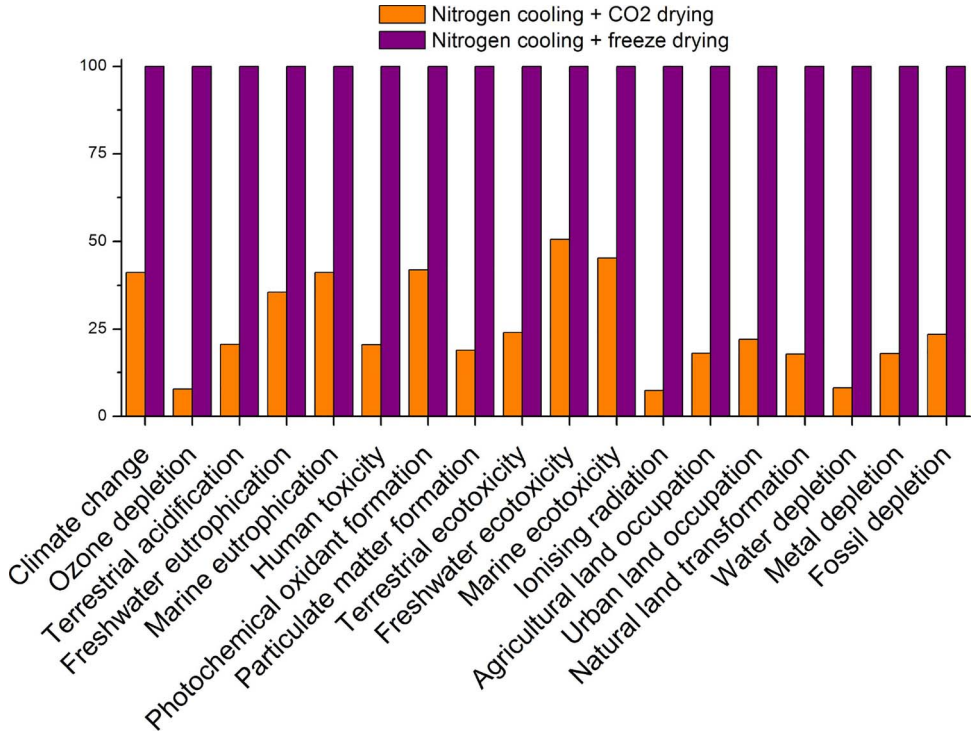

Fig. 14. Environmental impact assessment for the freeze-drying and SC-CO_2 drying technologies involved in the TIPS process.

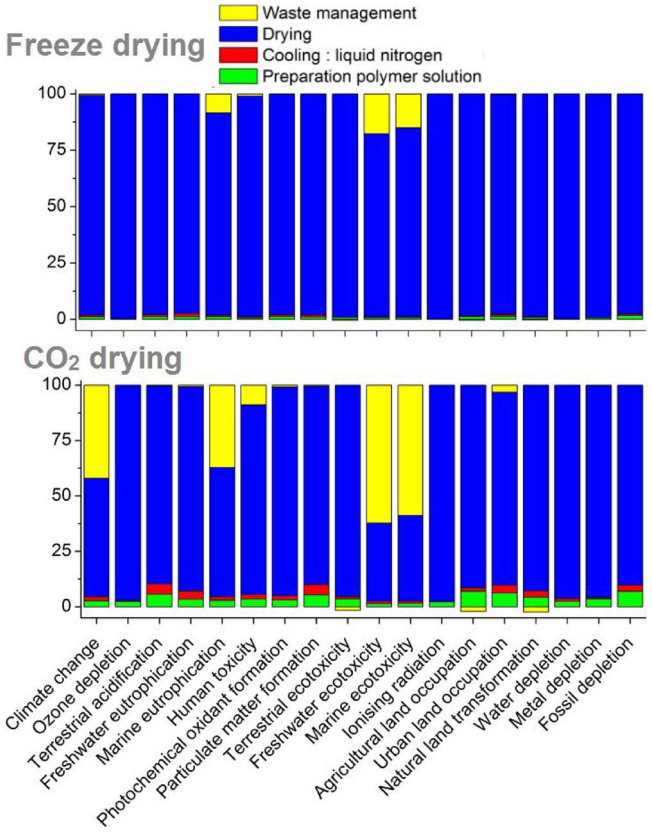

Fig. 15. Detailed environmental impact assessment considering the whole TIPS process with a nitrogen cooling (–196 °C) and a freeze-drying (upper histogram) or SC-CO_2 drying (lower histogram).

conducted on each drying technology to see the impact repartition depending on the process step (solution preparation, cooling, drying and waste management). As one can see in Fig. 15, the drying step was clearly the most damaging step in both cases with freeze-drying or SC-CO_2 drying. Considering SC-CO_2 drying, the electricity consumption (used for the production of SC-CO_2) was also quite important compared to the other steps of the process, while it represented less than 10% of the electricity used with freeze-drying.

Moreover, for most of the impact categories and for both scenarios, the second source was the management of generated wastes. Two main outputs of the process have been considered as wastes: the gases (CO_2 and nitrogen) and liquid chemicals (ethanol and 1,4-dioxane). As previously mentioned, the scaffolds end-of-life was not assessed here. In this study, it was considered that the gases were simply released to the atmosphere and liquids were sent to the French waste scenario. This explained the importance of waste management regarding the climate change, marine eutrophication and freshwater and marine ecotoxicity for the CO_2 drying alterative: 4 kg of CO_2 were emitted into the atmosphere for the production of each group of 50 scaffolds. However, other scenarios for waste management could be proposed. For example, the recycling of gaseous and liquid solvents could be considered. Unfortunately, a lack of data for these retreatment scenarios prevented a simulation in the SimaPro software but, at an industrial scale, the CO_2 used at the drying step would probably be recycled. In this way, an estimation conducted at lab scale led to the conclusion that 75% of liquid CO_2 could be saved. This would increase even more the interest of this technology against freeze-drying. These LCA results are all the more interesting because they could be transposed to many processes using freeze-drying that would be compatible with SC-CO_2.

4. Conclusion

Firstly, this study was focused on an in-depth parametric study of the TIPS process assisted by the SC-CO_2 technology and its scale-up for production of PLAs scaffolds. A systemic approach was deployed to study the effects of the major process key parameters such as polymer concentration, molecular weight, solvent miscibility, and cooling temperature on the scaffold characteristics and in relation to the tissue engineering applications. Moreover, the mechanical performances of scaffolds have been characterized. This helped to highlight the

relationship between process parameters, morphology and structure of the PLLA scaffolds and their behaviour under compressive stress. Besides, this work was the first known attempt to conduct an environmental analysis of TIPS process and the comparison between SC-CO_2 and freeze drying technologies. The results of the LCA have shown that the use of SC-CO_2 drying process was thriftier in energy than freeze drying process classically used, and reduced the environmental costs. Indeed, SC-CO_2 drying process made possible the reduction of between 50 and 90% of the environmental impacts of the whole process. Moreover the production time was also drastically reduced from several days to several hours. To conclude, this work has shown the potentiality (*i*) to transfer in industrial scale an eco-friendly process like TIPS assisted by supercritical CO_2 and (*ii*) to produce polymer scaffolds with suitable microstructures and mechanical properties for treatment of tissue and bone chronic disorders. In this way, it will be interesting to study the osteogenic, osteoconductive and osteoinductive potential of these PLLA scaffolds.

Conflicts of interest

There are no conflicts to declare.

Acknowledgements

The authors are grateful for the financial support from the MATIERES project and the "Région Pays de la Loire"(FRANCE). The authors thank the SCIAM *("Service Commun d'Imagerie et d'Analyse Microscopique",* University of Angers) for scanning electron microscopy images, the PIAM *("Plateforme d'Ingénierie et d'Analyses Moléculaires",* University of Angers) for DSC analyses, the BIA laboratory (INRA U1268, University of Nantes, France) for compressive tests.

Appendix A. Supplementary data

Supplementary data associated with this article can be found, in the online version, at https://doi.org/10.1016/j.supflu.2018.02.015.

References

[1] A. Salerno, M. Fernández-Gutiérrez, J. San Román del Barrio, C. Domingo, Bio-safe fabrication of PLA scaffolds for bone tissue engineering by combining phase separation, porogen leaching and scCO2 drying, J. Supercrit. Fluids 97 (2015) 238–246, http://dx.doi.org/10.1016/j.supflu.2014.10.029.

[2] M. Santoro, S.R. Shah, J.L. Walker, A.G. Mikos, Poly(lactic acid) nanofibrous scaffolds for tissue engineering, Adv. Drug Deliv. Rev. 107 (2016) 206–212, http://dx.doi.org/10.1016/j.addr.2016.04.019.

[3] S. Chen, Z. He, G. Xu, X. Xiao, Fabrication of nanofibrous tubular scaffolds for bone tissue engineering, Mater. Lett. Complete (2016) 289–293, http://dx.doi.org/10.1016/j.matlet.2016.07.015.

[4] T. Nie, L. Xue, M. Ge, H. Ma, J. Zhang, Fabrication of poly(L-lactic acid) tissue engineering scaffolds with precisely controlled gradient structure, Mater. Lett. Complete (2016) 25–28, http://dx.doi.org/10.1016/j.matlet.2016.04.078.

[5] Y. Elsayed, C. Lekakou, 2 – Designing and modeling pore size distribution in tissue scaffolds A2, in: Tomlins Paul (Ed.), Characterisation Des. Tissue Scaffolds, Woodhead Publishing, 2016, pp. 23–43, , http://dx.doi.org/10.1016/B978-1-78242-087-3.00002-X.

[6] J. Lee, M.J. Cuddihy, N.A. Kotov, Three-dimensional cell culture matrices: state of the art, Tissue Eng. Part B Rev. 14 (2008) 61–86, http://dx.doi.org/10.1089/teb.2007.0150.

[7] Y. Liu, J. Lim, S.-H. Teoh, Review: development of clinically relevant scaffolds for vascularised bone tissue engineering, Biotechnol. Adv. 31 (2013) 688–705, http://dx.doi.org/10.1016/j.biotechadv.2012.10.003.

[8] F.J. O'Brien, Biomaterials & scaffolds for tissue engineering, Mater. Today 14 (2011) 88–95, http://dx.doi.org/10.1016/S1369-7021(11)70058-X.

[9] D.W. Hutmacher, Scaffold design and fabrication technologies for engineering tissues–state of the art and future perspectives, J. Biomater. Sci. Polym. Ed. 12 (2001) 107–124.

[10] E. Reverchon, S. Cardea, Supercritical fluids in 3-D tissue engineering, J. Supercrit. Fluids 69 (2012) 97–107, http://dx.doi.org/10.1016/j.supflu.2012.05.010.

[11] J. Zhang, S.-G. Yang, J.-X. Ding, Z.-M. Li, Tailor-made poly(L-lactide)/poly(lactide-co-glycolide)/hydroxyapatite composite scaffolds prepared via high-pressure compression molding/salt leaching, RSC Adv. 6 (2016) 47418–47426, http://dx.doi.org/10.1039/C6RA06906A.

[12] J. Guan, K.L. Fujimoto, M.S. Sacks, W.R. Wagner, Preparation and characterization of highly porous, biodegradable polyurethane scaffolds for soft tissue applications, Biomaterials 26 (2005) 3961–3971, http://dx.doi.org/10.1016/j.biomaterials.2004.10.018.

[13] K. Whang, C.H. Thomas, K.E. Healy, G. Nuber, A novel method to fabricate bioabsorbable scaffolds, Polymer 36 (1995) 837–842, http://dx.doi.org/10.1016/0032-3861(95)93115-3.

[14] N. Sultana, M. Wang, Fabrication of HA/PHBV composite scaffolds through the emulsion freezing/freeze-drying process and characterisation of the scaffolds, J. Mater. Sci. Mater. Med. 19 (2007) 2555, http://dx.doi.org/10.1007/s10856-007-3214-3.

[15] J. An, J.E.M. Teoh, R. Suntornnond, C.K. Chua, Design and 3D printing of scaffolds and tissues, Engineering 1 (2015) 261–268, http://dx.doi.org/10.15302/J-ENG-2015061.

[16] L.J.M. Jacobs, M.F. Kemmere, J.T.F. Keurentjes, Sustainable polymer foaming using high pressure carbon dioxide: a review on fundamentals, processes and applications, Green Chem. 10 (2008) 731, http://dx.doi.org/10.1039/b801895b.

[17] C. Ji, N. Annabi, M. Hosseinkhani, S. Sivaloganathan, F. Dehghani, Fabrication of poly-DL-lactide/polyethylene glycol scaffolds using the gas foaming technique, Acta Biomater. 8 (2012) 570–578, http://dx.doi.org/10.1016/j.actbio.2011.09.028.

[18] F. Dehghani, N. Annabi, Engineering porous scaffolds using gas-based techniques, Curr. Opin. Biotechnol. 22 (2011) 661–666, http://dx.doi.org/10.1016/j.copbio.2011.04.005.

[19] S. Molladavoodi, M. Gorbet, J. Medley, H. Ju Kwon, Investigation of microstructure, mechanical properties and cellular viability of poly(l-lactic acid) tissue engineering scaffolds prepared by different thermally induced phase separation protocols, J. Mech. Behav. Biomed. Mater. 17 (2013) 186–197, http://dx.doi.org/10.1016/j.jmbbm.2012.08.021.

[20] G. Conoscenti, V.L. Carrubba, V. Brucato, A versatile technique to produce porous polymeric scaffolds: the thermally induced phase separation (TIPS) method, Arch. Chem. Res. 1 (2017), http://dx.doi.org/10.21767/2572-4657.100012.

[21] M. Flaibani, N. Elvassore, Gas anti-solvent precipitation assisted salt leaching for generation of micro- and nano-porous wall in bio-polymeric 3D scaffolds, Mater. Sci. Eng. C 32 (2012) 1632–1639, http://dx.doi.org/10.1016/j.msec.2012.04.054.

[22] F. Carfì Pavia, F.S. Palumbo, V. La Carrubba, F. Bongiovì, V. Brucato, G. Pitarresi, G. Giammona, Modulation of physical and biological properties of a composite PLLA and polyaspartamide derivative obtained via thermally induced phase separation (TIPS) technique, Mater. Sci. Eng. C Mater. Biol. Appl. 67 (2016) 561–569, http://dx.doi.org/10.1016/j.msec.2016.05.040.

[23] M. Okamoto, B. John, Synthetic biopolymer nanocomposites for tissue engineering scaffolds, Prog. Polym. Sci. 38 (2013) 1487–1503, http://dx.doi.org/10.1016/j.progpolymsci.2013.06.001.

[24] B.A.C. Harley, H.-D. Kim, M.H. Zaman, I.V. Yannas, D.A. Lauffenburger, L.J. Gibson, Microarchitecture of three-dimensional scaffolds influences cell migration behavior via junction interactions, Biophys. J. 95 (2008) 4013–4024, http://dx.doi.org/10.1529/biophysj.107.122598.

[25] V.L. Carrubba, F.C. Pavia, V. Brucato, S. Piccarolo, PLLA/PLA scaffolds prepared via Thermally Induced Phase Separation (TIPS): tuning of properties and biodegradability, Int. J. Mater. Form. 1 (2008) 619–622, http://dx.doi.org/10.1007/s12289-008-0332-5.

[26] R.A. Auras, L.-T. Lim, S.E.M. Selke, H. Tsuji, Poly(lactic Acid): Synthesis, Structures, Properties, Processing, and Applications, John Wiley & Sons, 2011.

[27] C. Schugens, V. Maquet, C. Grandfils, R. Jerome, P. Teyssie, Biodegradable and macroporous polylactide implants for cell transplantation: 1. Preparation of macroporous polylactide supports by solid-liquid phase separationn, Polymer 37 (1996) 1027–1038, http://dx.doi.org/10.1016/0032-3861(96)87287-9.

[28] C. Schugens, V. Maquet, C. Grandfils, R. Jerome, P. Teyssie, Polylactide macroporous biodegradable implants for cell transplantation. II. Preparation of polylactide foams by liquid–liquid phase separation, J. Biomed. Mater. Res. 30 (1996) 449–461, http://dx.doi.org/10.1002/(SICI)1097-4636(199604)30:4<449:AID-JBM3>3.0.CO;2-P.

[29] Y.S. Nam, T.G. Park, Biodegradable polymeric microcellular foams by modified thermally induced phase separation method, Biomaterials 20 (1999) 1783–1790, http://dx.doi.org/10.1016/S0142-9612(99)00073-3.

[30] J.-S. Chen, S.-L. Tu, R.-Y. Tsay, A morphological study of porous polylactide scaffolds prepared by thermally induced phase separation, J. Taiwan Inst. Chem. Eng. 41 (2010) 229–238, http://dx.doi.org/10.1016/j.jtice.2009.08.008.

[31] P.X. Ma, R. Zhang, Synthetic nano-scale fibrous extracellular matrix, J. Biomed. Mater. Res. 46 (1999) 60–72.

[32] L. He, Y. Zhang, X. Zeng, D. Quan, S. Liao, Y. Zeng, J. Lu, S. Ramakrishna, Fabrication and characterization of poly(L-lactic acid) 3D nanofibrous scaffolds with controlled architecture by liquid–liquid phase separation from a ternary polymer–solvent system, Polymer 50 (2009) 4128–4138, http://dx.doi.org/10.1016/j.polymer.2009.06.025.

[33] A. Salerno, C. Domingo, Making microporous nanometre-scale fibrous PLA aerogels with clean and reliable supercritical CO2 based approaches, Microporous Mesoporous Mat. 184 (2014) 162–168, http://dx.doi.org/10.1016/j.micromeso.2013.10.019.

[34] E. Reverchon, S. Cardea, C. Rapuano, A new supercritical fluid-based process to produce scaffolds for tissue replacement, J. Supercrit. Fluids 45 (2008) 365–373, http://dx.doi.org/10.1016/j.supflu.2008.01.005.

[35] S. Huebschmann, D. Kralisch, H. Loewe, D. Breuch, J.H. Petersen, T. Dietrich, R. Scholz, Decision support towards agile eco-design of microreaction processes by accompanying (simplified) life cycle assessment, Green Chem. 13 (2011) 1694, http://dx.doi.org/10.1039/c1gc15054e.

[36] E.T.H. Vink, S. Davies, Life cycle inventory and impact assessment datafor 2014 IngeoTM polylactide production, Ind. Biotechnol. 11 (2015) 167–180, http://dx.

doi.org/10.1089/ind.2015.0003.
[37] M.R. Yates, C.Y. Barlow, Life cycle assessments of biodegradable, commercial biopolymers—a critical review, Resour. Conserv. Recycl. 78 (2013) 54–66, http://dx.doi.org/10.1016/j.resconrec.2013.06.010.
[38] E.T.H. Vink, K.R. Rábago, D.A. Glassner, P.R. Gruber, Applications of life cycle assessment to NatureWorksTM polylactide (PLA) production, Polym. Degrad. Stab. 80 (2003) 403–419, http://dx.doi.org/10.1016/S0141-3910(02)00372-5.
[39] Y. Wang, Y.-X. Gao, J. Song, M. Bonin, M. Guo, R. Murphy, Assessment of technical and environmental performances of wheat-based foams in thermal packaging applications, Packag. Technol. Sci. 23 (2010) 363–382, http://dx.doi.org/10.1002/pts.897.
[40] F. Gironi, V. Piemonte, Life cycle assessment of polylactic acid and polyethylene terephthalate bottles for drinking water, Environ. Prog. Sustain. Energy 30 (2011) 459–468, http://dx.doi.org/10.1002/ep.10490.
[41] U. Suwanmanee, V. Varabuntoonvit, P. Chaiwutthinan, M. Tajan, T. Mungcharoen, T. Leejarkpai, Life cycle assessment of single use thermoform boxes made from polystyrene (PS), polylactic acid, (PLA), and PLA/starch: cradle to consumer gate, Int. J. Life Cycle Assess 18 (2012) 401–417, http://dx.doi.org/10.1007/s11367-012-0479-7.
[42] X. Su, Z. Luo, Y. Li, C. Huang, Life cycle inventory comparison of different building insulation materials and uncertainty analysis, J. Clean. Prod. 1 (Part 1) (2016) 275–281, http://dx.doi.org/10.1016/j.jclepro.2015.08.113.
[43] F. Ardente, M. Beccali, M. Cellura, M. Mistretta, Building energy performance: a LCA case study of kenaf-fibres insulation board, Energy Build. 40 (2008) 1–10, http://dx.doi.org/10.1016/j.enbuild.2006.12.009.
[44] I. Zabalza Bribián, A. Valero Capilla, A. Aranda Usón, Life cycle assessment of building materials: comparative analysis of energy and environmental impacts and evaluation of the eco-efficiency improvement potential, Build. Environ. 46 (2011) 1133–1140, http://dx.doi.org/10.1016/j.buildenv.2010.12.002.
[45] C. Sardo, B. Nottelet, D. Triolo, G. Giammona, X. Garric, J.-P. Lavigne, G. Cavallaro, J. Coudane, When functionalization of PLA surfaces meets Thiol–Yne photochemistry: case study with antibacterial polyaspartamide derivatives, Biomacromolecules 15 (2014) 4351–4362, http://dx.doi.org/10.1021/bm5013772.
[46] M. Pyda, R. Bopp, B. Wunderlich, Heat capacity of poly(lactic acid), J. Chem. Thermodyn. 36 (2004) 731–742, http://dx.doi.org/10.1016/j.jct.2004.05.003.
[47] F.J. Hua, T.G. Park, D.S. Lee, A facile preparation of highly interconnected macroporous poly(d,L-lactic acid-co-glycolic acid) (PLGA) scaffolds by liquid–liquid phase separation of a PLGA–dioxane–water ternary system, Polymer 44 (2003) 1911–1920, http://dx.doi.org/10.1016/S0032-3861(03)00025-9.
[48] C.A. Schneider, W.S. Rasband, K.W. Eliceiri, NIH Image to ImageJ: 25 years of image analysis, Nat. Methods 9 (2012) 671–675, http://dx.doi.org/10.1038/nmeth.2089.
[49] NF EN ISO 14040 (2006-10) − Management environnemental − Analyse du cycle de vie − Principes et cadre, n.d.
[50] S. Cardea, L. Baldino, P. Pisanti, E. Reverchon, 3-D PLLA scaffolds formation by a supercritical freeze extraction assisted process, J. Mater. Sci. Mater. Med. 25 (2014) 355–362, http://dx.doi.org/10.1007/s10856-013-5069-0.
[51] I. Tsivintzelis, S.I. Marras, I. Zuburtikudis, C. Panayiotou, Porous poly(L-lactic acid) nanocomposite scaffolds prepared by phase inversion using supercritical CO2 as antisolvent, Polymer 48 (2007) 6311–6318, http://dx.doi.org/10.1016/j.polymer.2007.08.021.
[52] F.J. Hua, G.E. Kim, J.D. Lee, Y.K. Son, D.S. Lee, Macroporous poly(L-lactide) scaffold 1. Preparation of a macroporous scaffold by liquid–liquid phase separation of a PLLA–dioxane–water system, J. Biomed. Mater. Res. 63 (2002) 161–167.
[53] H.L. Frisch, Diffusion in polymers, in: J. Crank, G.S. Park (Eds.), J. Appl. Polym. Sci. vol. 14, Academic Press, London and New York, 1970, , http://dx.doi.org/10.1002/app.1970.070140623.
[54] Q.L. Loh, C. Choong, Three-dimensional scaffolds for tissue engineering applications: role of porosity and pore size, Tissue Eng. Part B Rev. 19 (2013) 485–502, http://dx.doi.org/10.1089/ten.TEB.2012.0437.
[55] L. Polo-Corrales, M. Latorre-Esteves, J.E. Ramirez-Vick, Scaffold design for bone regeneration, J. Nanosci. Nanotechnol. 14 (2014) 15–56.
[56] F. Yang, X. Qu, W. Cui, J. Bei, F. Yu, S. Lu, S. Wang, Manufacturing and morphology structure of polylactide-type microtubules orientation-structured scaffolds, Biomaterials 27 (2006) 4923–4933, http://dx.doi.org/10.1016/j.biomaterials.2006.05.028.
[57] D. Odedra, L. Chiu, L. Reis, F. Rask, K. Chiang, M. Radisic, Cardiac tissue engineering, Biomater. Tissue Eng. Appl. Springer Vienna (2011) 421–456, http://dx.doi.org/10.1007/978-3-7091-0385-2_15.
[58] Y. Wang, J. Hu, J. Jiao, Z. Liu, Z. Zhou, C. Zhao, L.-J. Chang, Y.E. Chen, P.X. Ma, B. Yang, Engineering vascular tissue with functional smooth muscle cells derived from human iPS cells and nanofibrous scaffolds, Biomaterials 35 (2014) 8960–8969, http://dx.doi.org/10.1016/j.biomaterials.2014.07.011.
[59] J. Zeltinger, J.K. Sherwood, D.A. Graham, R. Müeller, L.G. Griffith, Effect of pore size and void fraction on cellular adhesion, proliferation, and matrix deposition, Tissue Eng. 7 (2001) 557–572, http://dx.doi.org/10.1089/107632701753213183.
[60] S. Yang, K.-F. Leong, Z. Du, C.-K. Chua, The Design of Scaffolds for Use in Tissue Engineering. Part I. Traditional Factors, Tissue Eng. 7 (2001) 679–689, http://dx.doi.org/10.1089/107632701753337645.
[61] R. Liu, K. Li, M. Liu, Y. Liu, H. Liu, Free poly(L-lactic acid) spherulites grown from thermally induced phase separation and crystallization kinetics, J. Polym. Sci. Part B Polym. Phys. 52 (2014) 1476–1489, http://dx.doi.org/10.1002/polb.23587.
[62] W. Zhang, M. Liu, Y. Liu, R. Liu, F. Wei, R. Xiao, H. Liu, 3D porous poly(L-lactic acid) foams composed of nanofibers, nanofibrous microsheaves and microspheres and their application in oil–water separation, J. Mater. Chem. A 3 (2015) 14054–14062, http://dx.doi.org/10.1039/C5TA02759D.
[63] K.M. Woo, V.J. Chen, P.X. Ma, Nano-fibrous scaffolding architecture selectively enhances protein adsorption contributing to cell attachment, J. Biomed. Mater. Res. A 67A (2003) 531–537, http://dx.doi.org/10.1002/jbm.a.10098.
[64] I. Bružauskaitė, D. Bironaitė, E. Bagdonas, E. Bernotienė, Scaffolds and cells for tissue regeneration: different scaffold pore sizes-different cell effects, Cytotechnology 68 (2016) 355–369, http://dx.doi.org/10.1007/s10616-015-9895-4.
[65] N.C. Hilyard, A. Cunningham, Low Density Cellular Plastics: Physical Basis of Behaviour, Springer Science & Business Media, 2012.
[66] K. Rezwan, Q.Z. Chen, J.J. Blaker, A.R. Boccaccini, Biodegradable and bioactive porous polymer/inorganic composite scaffolds for bone tissue engineering, Biomaterials 27 (2006) 3413–3431, http://dx.doi.org/10.1016/j.biomaterials.2006.01.039.
[67] F. Carrasco, P. Pagès, J. Gámez-Pérez, O.O. Santana, M.L. Maspoch, Processing of poly(lactic acid): characterization of chemical structure, thermal stability and mechanical properties, Polym. Degrad. Stab. 95 (2010) 116–125, http://dx.doi.org/10.1016/j.polymdegradstab.2009.11.045.
[68] A.M. Harris, E.C. Lee, Improving mechanical performance of injection molded PLA by controlling crystallinity, J. Appl. Polym. Sci. 107 (2008) 2246–2255, http://dx.doi.org/10.1002/app.27261.
[69] G. Perego, G.D. Cella, C. Bastioli, Effect of molecular weight and crystallinity on poly(lactic acid) mechanical properties, J. Appl. Polym. Sci. 59 (1996) 37–43, http://dx.doi.org/10.1002/(SICI)1097-4628(19960103)59:1<37:AID-APP6>3.0.CO;2-N.
[70] J.M. Mansour, Biomechanics of cartilage, Kinesiol. Mech. Pathomechanics Hum. Mov (2013) 69–83 https://cwru.pure.elsevier.com/en/publications/biomechanics-of-cartilage (Accessed October 24 2017) second ed..
[71] P.S. Patel, D.E. Shepherd, D.W. Hukins, Compressive properties of commercially available polyurethane foams as mechanical models for osteoporotic human cancellous bone, BMC Musculoskelet Disord. 9 (2008) 137, http://dx.doi.org/10.1186/1471-2474-9-137.
[72] É. Lakatos, L. Magyar, I. Bojtár, Material properties of the mandibular trabecular bone, J. Med. Eng. 2014 (2014) 7, http://dx.doi.org/10.1155/2014/470539 Article ID 470539.
[73] T. Beuvier, B. Calvignac, G. Jean-Robert Delcroix, M. Kien Tran, S. Kodjikian, N. Delorme, J.-F. Bardeau, A. Gibaud, F. Boury, Synthesis of hollow vaterite CaCO3 microspheres in supercritical carbon dioxide medium, J. Mater. Chem. 21 (2011) 9757–9761, http://dx.doi.org/10.1039/C1JM10770D.
[74] E. Chavez, T. Beuvier, M. Fernández, L. Hassani, B. Calvignac, F. Boury, A. Gibaud, Small-angle X-ray scattering analysis of porous powders of CaCO3, J. Appl. Crystallogr. 45 (2012), http://dx.doi.org/10.1107/S0021889812032219.
[75] M.-K. Tran, L.N. Hassani, B. Calvignac, T. Beuvier, F. Hindré, F. Boury, Lysozyme encapsulation within PLGA and CaCO3 microparticles using supercritical CO2 medium, J. Supercrit. Fluids 79 (2013) 159–169, http://dx.doi.org/10.1016/j.supflu.2013.02.024.
[76] L.N. Hassani, F. Hindré, T. Beuvier, B. Calvignac, N. Lautram, A. Gibaud, F. Boury, Lysozyme encapsulation into nanostructured CaCO3 microparticles using a supercritical CO2 process and comparison with the normal route, J. Mater. Chem. B 1 (2013) 4011–4019, http://dx.doi.org/10.1039/C3TB20467G.
[77] V.E. Bosio, M.L. Cacicedo, B. Calvignac, I. León, T. Beuvier, F. Boury, G.R. Castro, Synthesis and characterization of CaCO3-biopolymer hybrid nanoporous microparticles for controlled release of doxorubicin, Colloids Surf. B Biointerfaces 123 (2014) 158–169, http://dx.doi.org/10.1016/j.colsurfb.2014.09.011.
[78] E.Y. Zeynep, D. Antoine, C. Brice, B. Frank, J. Christine, Double hydrophilic polyphosphoester containing copolymers as efficient templating agents for calcium carbonate microparticles, J. Mater. Chem. B 3 (2015) 7227–7236, http://dx.doi.org/10.1039/C5TB00887E.
[79] Z. Ergul Yilmaz, T. Cordonnier, A. Debuigne, B. Calvignac, C. Jerome, F. Boury, Protein encapsulation and release from PEO-b-polyphosphoester templated calcium carbonate particles, Int. J. Pharm. 513 (2016) 130–137, http://dx.doi.org/10.1016/j.ijpharm.2016.09.007.
[80] R.A. Yukna, Clinical evaluation of coralline calcium carbonate as a bone replacement graft material in human periodontal osseous defects, J. Periodontol. 65 (1994) 177–185, http://dx.doi.org/10.1902/jop.1994.65.2.177.
[81] F. Soost, B. Reisshauer, A. Herrmann, H.J. Neumann, Natural coral calcium carbonate as alternative substitute in bone defects of the skull, Mund- Kiefer-Gesichtschirurgie MKG 2 (1998) 96–100, http://dx.doi.org/10.1007/s100060050037.
[82] M.G. Gandolfi, F. Zamparini, M. Degli Esposti, F. Chiellini, C. Aparicio, F. Fava, P. Fabbri, P. Taddei, C. Prati, Polylactic acid-based porous scaffolds doped with calcium silicate and dicalcium phosphate dihydrate designed for biomedical application, Mater. Sci. Eng. C 82 (2018) 163–181, http://dx.doi.org/10.1016/j.msec.2017.08.040.
[83] J.-S. Chen, S.-L. Tu, R.-Y. Tsay, A morphological study of porous polylactide scaffolds prepared by thermally induced phase separation, J. Taiwan Inst. Chem. Eng. 41 (2010) 229–238, http://dx.doi.org/10.1016/j.jtice.2009.08.008.